

# SSCHA-based evolutionary crystal structure prediction at finite temperatures with account for quantum nuclear motion

Daniil Poletaev\*, Artem Oganov

Materials Discovery Laboratory, Skolkovo Institute of Science and Technology, 121205 Moscow, Russia

## Abstract

Accurate crystal structure prediction (CSP) at finite temperatures with quantum anharmonic effects remains challenging but very prominent in systems with lightweight atoms such as superconducting hydrides. In this work, we integrate machine-learned interatomic potentials (MLIPs) with the stochastic self-consistent harmonic approximation (SSCHA) to enable evolutionary CSP on the quantum anharmonic free-energy landscape. Using  $\text{LaH}_{10}$  at 150 GPa and 300 K as a test case, we compare two approaches for SSCHA-based CSP: using light-weight active-learning MLIPs (AL-MLIPs) trained on-the-fly from scratch, and foundation models or universal MLIPs (uMLIPs) from the Matbench project. We demonstrate that AL-MLIPs allow to correctly predict the experimentally known cubic  $\text{Fm}\bar{3}\text{m}$  phase as the most stable polymorph at 150 GPa but require corrections within the thermodynamic perturbation theory to get consistent results. The uMLIP Mattersim-5m allow to conduct SSCHA-based CSP without requiring per-structure training and even get correct structure ranking near the global minimum, though fine-tuning may be needed for higher accuracy. Our results show that including quantum anharmonicity simplifies the free-energy landscape and is essential for correct stability rankings, that is especially important for high-temperature phases that could be missed in classical 0 K CSP. The proposed approach extends the reach of CSP to systems where quantum nuclear motion and anharmonicity dominate.

## Keywords:

crystal structure prediction, structure ranking at finite temperature, quantum anharmonicity, La-H, thermodynamic perturbation theory, USPEX, moment tensor potentials, active learning, universal MLIPs, superconducting hydrides

## 1. Introduction

Accurate prediction of crystal structures at various pressures and temperatures is crucial for materials discovery and design [1, 2]. The success of structure prediction depends critically on correctly solving the structure ranking problem [2]. While state-of-the-art *ab initio* methods, e.g. density functional theory (DFT) and post-DFT methods provide the highest accuracy for structure ranking at 0 K, their computational cost severely limits applications at finite temperatures [1–6]. Most computational searches therefore rely on structure ranking exclusively at 0 K [3, 7].

T-USPEX was developed to overcome these limitations by enabling finite-temperature structure prediction using classical molecular dynamics (MD) with semi-empirical or machine-learning interatomic potentials (MLIPs) for structure relaxation, sampling phase space, and free energy calculation combined with pressure and free energy corrections within the thermodynamic perturbation theory for ensuring structure ranking at *ab initio* level [7]. However, classical MD is unsuitable for materials with strong quantum anharmonic effects. Many systems, particularly superconducting hydrides [8–11], charge-density-wave materials [12, 13], and thermoelectric compounds [14], exhibit quantum anharmonicity that critically influences

thermodynamic stability and material properties both at 0 K and finite temperatures.

The stochastic self-consistent harmonic approximation (SSCHA) provides a rigorous framework for treating quantum anharmonic effects [9, 14, 15]. However, the computational cost of SSCHA restricts its direct use in structure prediction. *Ab initio*-based structure optimization within SSCHA can take weeks to months, whereas hundreds to thousands of such optimizations are usually required [2].

Active-learning MLIPs (AL-MLIPs) offer a promising solution for accelerating SSCHA calculations [13, 16–20]. When integrated with structure prediction, AL-MLIPs can dramatically reduce the cost of SSCHA relaxations while preserving the accuracy needed to model quantum anharmonicity at *ab initio*-level. Moreover, the recent development of universal MLIPs (uMLIPs), also known as large atomistic models or foundation models [21], presents a further opportunity to make crystal structure prediction (CSP) with quantum anharmonic effects more feasible.

In this work, we integrate both AL-MLIPs and uMLIPs into the SSCHA-based structure prediction within USPEX [1, 2]. Using  $\text{LaH}_{10}$  at 150 GPa as a validation case where phase stability is controlled by quantum anharmonicity, we compare evolutionary CSP on the quantum anharmonic free energy landscape using both AL-MLIPs and uMLIPs.

$\text{LaH}_{10}$  have been extensively studied both theoretically and

\*Corresponding author: D.O. Poletaev.

experimentally [10, 22–33], enabling robust validation of our CSP results. The cubic  $Fm\bar{3}m$  phase of  $LaH_{10}$  with sodalite-like structure was first theoretically predicted at pressures  $\geq 150$  GPa [22, 23] and was found experimentally to be stable at pressures above 135–140 GPa [29, 32, 33]. Theoretical studies at different levels of theory have revealed that accounting for anharmonic effects is essential: while the cubic phase appears dynamically unstable within the harmonic approximation at pressures below 210–230 GPa, anharmonic effects stabilize it at pressures of 129–150 GPa [10, 24, 25].

## 2. Results and discussion

### 2.1. CSP of the most stable $LaH_{10}$ polymorph on the quantum anharmonic free energy landscape with AL-MLIPs

We performed two independent searches for the most stable structure of  $LaH_{10}$  on the quantum anharmonic free energy landscape at 150 GPa and 300 K using AL-MLIPs. In the first search, for each structure proposed by USPEX we trained a separate MLIP from scratch during the SSCHA relaxation. In the second search, before the MLIP training, we evaluated whether any existing MLIPs from previous relaxations were better suited for a new structure than initializing a new one. The MLIP needing the fewest structures for retraining was selected and used for relaxation within the SSCHA. If further refinement was necessary, the selected MLIP was retrained. The details of training of AL-MLIPs during the structure search and of the SSCHA relaxation are in the Section 5.2 and 5.3 and in the Supplementary Materials.

With AL-MLIPs trained from scratch for each structure, USPEX predicted only three different phases of  $LaH_{10}$  on the anharmonic free energy landscape. The crystallographic information about these phases and visualization of their lattices can be found in Table 1 and Figure 1.

Table 1: Crystallographic information about three  $LaH_{10}$  phases predicted on the anharmonic free energy landscape at 150 GPa and 300 K with AL-MLIPs trained from scratch for each structure. Fitness is a value of the free energy with respect to the ground state at the given conditions.

Phase	Fitness (eV/atom)	Lattice parameters	Atom coordinates (Wyckoff positions)		
$Fm\bar{3}m$	0	$a = 5.120 \text{ \AA}$	La	0.0	0.0
			H	0.25	0.25
			H	0.38	0.38
$Cmmm$	0.085	$a = 2.932 \text{ \AA}$ $b = 7.020 \text{ \AA}$ $c = 3.276 \text{ \AA}$	La	0.0	0.0
			H	0.0	0.295
			H	0.0	0.421
			H	0.168	0.172
$P6/mmm$	0.160	$a = 3.248 \text{ \AA}$ $c = 3.735 \text{ \AA}$	La	0.0	0.0
			H	0.333	0.667
			H	0.314	0.0

The most stable predicted polymorph has the cubic  $Fm\bar{3}m$  symmetry in accordance with the experimental data [31] and it already appeared in the first generation. It should be noted that *before* the SSCHA relaxation this polymorph had the lower symmetry ( $I\bar{m}mm$ ), i.e., in the structure prediction results on the classical energy landscape at 0 K it would appear as an  $I\bar{m}mm$  structure, not  $Fm\bar{3}m$ . In the subsequent generations,

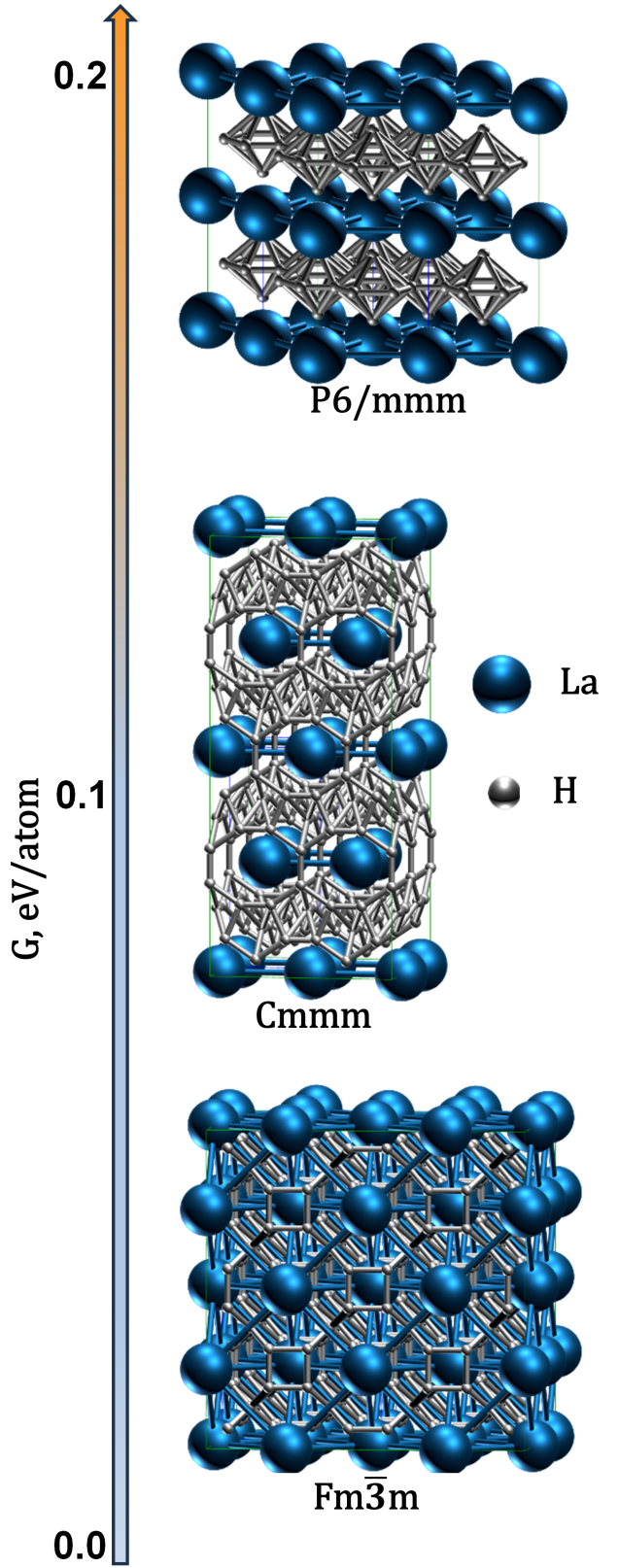


Figure 1: Three  $LaH_{10}$  polymorphs with  $Fm\bar{3}m$ ,  $Cmmm$ , and  $P6/mmm$  space-groups predicted on the anharmonic free energy landscape at 300 K and 150 GPa with AL-MLIPs trained from scratch for each structure. The values of the free energy,  $G$ , are with respect to the ground state structure,  $Fm\bar{3}m$ . The visualizations of crystal structures were prepared with STMng program [34].

cubic  $Fm\bar{3}m$   $\text{LaH}_{10}$  was obtained several times after the SS-CHA relaxations from structures with  $P\bar{1}$ ,  $C2$ ,  $C2/m$ ,  $Immm$ ,  $I4/mmm$ ,  $R\bar{3}m$ , and  $Fm\bar{3}m$  symmetry groups on classical energy landscape. The calculated lattice parameter for cubic  $\text{LaH}_{10}$  (5.120 Å) shows a slight deviation from the experimental value (5.102 Å) measured at 150 GPa [31]. This minor discrepancy can likely be attributed to a different hydrogen content, as the experimental sample in [31] was proposed to have a composition closer to  $\text{LaH}_{9.6}$ .

The second  $\text{LaH}_{10}$  structure predicted on the anharmonic free energy landscape has orthorhombic  $Cmmm$  symmetry and around 85 meV/atom higher Gibbs free energy at 300 K than cubic  $Fm\bar{3}m$  structure. It was obtained from structures with  $P1$  and  $Cmmm$  spacegroups emerged on classical energy landscape. The third predicted  $\text{LaH}_{10}$  polymorph has hexagonal layered-like structure with  $P6/mmm$  spacegroup. It was relaxed within the SSCHA from the  $P6/mm$  structure, and lies around 160 meV/atom higher than the ground-state. This hexagonal structure is similar to  $\text{LaH}_{16}$  structure with the same symmetry group that predicted earlier in the work of our group also at 150 GPa [25]. The difference of  $P6/mmm$   $\text{LaH}_{10}$  from  $\text{LaH}_{16}$  is in the hydrogen network between the layers.

The phonon dispersions clearly show that the lowest-energy cubic  $Fm\bar{3}m$  polymorph is dynamically stabilized by anharmonic lattice vibrations, consistent with previous literature [10, 33] (see Figure 2). In contrast, the higher-energy orthorhombic  $Cmmm$  and hexagonal  $P6/mmm$  polymorphs are dynamically stable both harmonically and anharmonically.

The CSP for the most stable  $\text{LaH}_{10}$  polymorph employing reusable AL-MLIPs yielded results nearly identical to those obtained with AL-MLIPs trained from scratch. USPEX successfully predicted the  $Fm\bar{3}m$  and  $Cmmm$  structures on the anharmonic free-energy landscape. However, the hexagonal  $P6/mmm$  structure was not predicted. This is expected, as evolutionary algorithms narrow the search space with each generation, and high-energy structures typically only appear from random initializations. This underscores the importance of structure prediction on finite-temperature free-energy landscapes, as this is the only way to identify structures that are far from the 0 K ground state but may be stabilized at higher temperatures.

The advantage of reusing AL-MLIPs is in reducing the number of DFT calculations needed for retraining. The ratio of total MLIP evaluations (energies, forces, and stresses) during SS-CHA relaxations to the total number of DFT calculations required for retraining was greater than 2000 for reusable AL-MLIPs, compared to only  $\sim 600$  for MLIPs trained from scratch representing a reduction in DFT calculations by a factor of more than three.

We also encountered pitfalls when employing reusable AL-MLIPs, which highlight two important considerations. First, repeatedly retraining a light-weight AL-MLIP on a continuously updated dataset can lead to accumulated training errors. These errors degrade the model’s predictions of energies, forces, and stresses for the perturbed configurations generated during SS-CHA relaxations. Consequently, some structures may be relaxed into the false metastable state on anharmonic free energy landscape. In our case, this led to the prediction of false

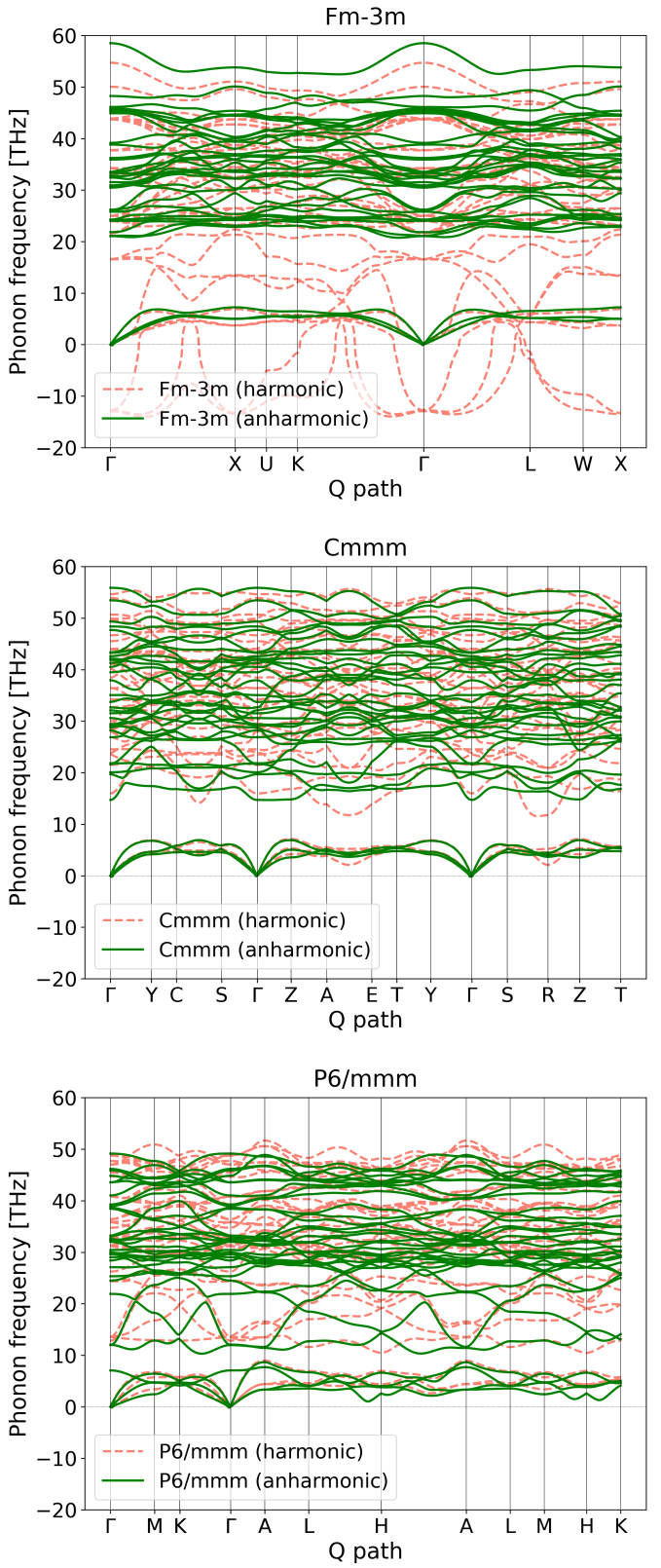


Figure 2: Harmonic and anharmonic phonon dispersion curves at 150 GPa for cubic  $\text{LaH}_{10}$  with  $Fm\bar{3}m$  symmetry group, orthorhombic  $\text{LaH}_{10}$  with  $Cmmm$  symmetry group, and hexagonal  $\text{LaH}_{10}$  with  $P6/mmm$  symmetry group.

metastable  $\text{LaH}_{10}$  structures with  $C2/m$  and  $R3m$  space groups, with energies approximately 110 meV/atom and 126 meV/atom above the ground state, respectively. Subsequent SSCHA relaxation of these structures with AL-MLIPs trained from scratch caused both to transform into the cubic  $\text{Fm}\bar{3}m$  structure.

The second point is that without corrections from thermodynamic perturbation theory [7, 35–37], the divergence in the calculated free energies for ostensibly identical structures can exceed 100 meV/atom. Applying these corrections reduces the divergence to a few meV/atom, which is acceptable when the free energy differences between unique predicted structures are on the order of tens of meV/atom, as is the case for  $\text{LaH}_{10}$ . For comparison, with AL-MLIPs trained from scratch for each structure, the free energy divergence for the same structures was no more than 20 meV/atom without corrections and was reduced to less than 1 meV/atom after corrections were applied. Thus, applying corrections for pressure and free energy within the thermodynamic perturbation theory is essential when employing reusable AL-MLIPs which tend to accumulate generalization errors as in our case.

## 2.2. CSP of the most stable $\text{LaH}_{10}$ polymorph on the quantum anharmonic free energy landscape with uMLIPs

In this work, we considered several uMLIPs from the Mat-bench discovery project [21] for use in high-pressure CSP on anharmonic free energy landscape. The candidates included CHGNet [38], DPA3 [39], GRACE [40], MACE [41], Mattersim-5m [42], OrbNet-v2 [43], and Sevennet [44].

Before conducting the finite-temperature CSP, we qualitatively evaluated each potential by relaxing the rhombohedral ( $\text{R}\bar{3}m$ )  $\text{LaH}_{10}$  structure within the SSCHA at 150 GPa and 300 K. With good potential, it should transform into the cubic ( $\text{Fm}\bar{3}m$ ) structure. Only three uMLIPs, namely CHGNet, MACE, and Mattersim-5m, successfully completed the SSCHA relaxation at the given conditions without failing due to unphysical atomic configurations. Among these, only Mattersim-5m relaxed the structure into the experimentally known stable cubic phase ( $\text{Fm}\bar{3}m$ ). Based on these results, we selected Mattersim-5m for further testing in CSP on anharmonic free-energy landscape of  $\text{LaH}_{10}$  at 150 GPa and 300 K using USPEX.

In the subsequent SSCHA-based, Mattersim-powered USPEX search, the cubic  $\text{Fm}\bar{3}m$  structure emerged in the first generation, consistent with previous searches using AL-MLIPs. It appeared multiple times, evolving from initial structures with both lower ( $\text{Fmmm}$ ,  $\text{Immm}$ ,  $\text{I}\bar{4}\text{m}2$ ,  $\text{Cm}$ ) and the same ( $\text{Fm}\bar{3}m$ ) symmetry. The free energy of this cubic phase was the lowest among all converged structures.

The second-ranked structure identified by Mattersim-5m on the anharmonic landscape has  $\text{Cmmm}$  symmetry, identical to one found with AL-MLIPs. However, Mattersim-5m placed this structure closer to the ground state (26 meV/atom above it, compared to 85 meV/atom with AL-MLIPs). Several other structures with symmetries  $\text{C}2/\text{m}$ ,  $\text{Immm}$ ,  $\text{R}3\text{m}$ ,  $\text{P}2/\text{m}$ ,  $\text{C}222$ , and  $\text{P}4/\text{mmm}$  were also found on the anharmonic free energy landscape with Mattersim-5m. Most of them, excluding  $\text{C}222$  and  $\text{P}4/\text{mmm}$ , have free energies within 100 meV/atom above the ground state. Likely, these structures represent false

metastable states on the anharmonic free-energy landscape, due to the insufficient accuracy of Mattersim-5m for the La-H system at 150 GPa, since we did not fine-tune this foundation model.

Overall, we found that the Mattersim-5m uMLIP can robustly guide SSCHA relaxations during CSP at high pressures, nearly eliminating the need to train AL-MLIPs from scratch. Moreover, with Mattersim-5m, roughly 90% of structures pre-relaxed at 0 K on the classical energy landscape also converged within the SSCHA at 300 K. In contrast, using AL-MLIPs (level eight MTPs) led to convergence for only about 30% of such structures. Another benefit is that thermodynamic perturbation corrections are less essential when using Mattersim-5m than with lightweight AL-MLIPs. For lightweight AL-MLIPs, these corrections are necessary to ensure consistent free energies across different relaxation paths. In contrast, with Mattersim-5m, the free energy of a converged SSCHA configuration is independent of its starting structure; corrections here are required not for internal consistency, but to align the free energy landscape with the ab initio reference. Note that in this work we did not apply thermodynamic perturbation theory corrections during SSCHA-based CSP with Mattersim-5m, yet we still obtained the correct free energy ranking for the two lowest-energy structures.

## 3. Discussion

In this work, we conducted three independent searches for the most stable  $\text{LaH}_{10}$  polymorph on the quantum anharmonic free energy landscape using different MLIP schemes. We relaxed all structures including high-energy ones on the quantum anharmonic free energy landscape, enabling a fully anharmonic CSP where the evolutionary algorithm selected structures for the next generation based on 300 K free energies rather than 0 K enthalpies. However, this SSCHA-based CSP required about two orders of magnitude more time than 0 K CSP, even with a ready-to-use uMLIP such as Mattersim-5m.

A more computationally efficient alternative could be to perform CSP on the classical energy landscape and then select most diverse low-enthalpy configurations for SSCHA relaxation. Recently, Gao et al. [45] proposed an iterative framework combining an evolutionary algorithm, a fine-tuned atomic foundation model (Mattersim-1m), and SSCHA relaxations, validated on  $\text{H}_3\text{S}$  phase stabilities. After fine-tuning Mattersim-1m, they performed classical CSP at 0 K and relaxed only the 100 lowest-enthalpy structures with SSCHA. Their comparison of classical and quantum anharmonic enthalpies for  $\text{H}_3\text{S}$  suggested that anharmonic effects dominate mainly in low-enthalpy structures, implying that relaxing only these selected configurations may be sufficient even for highly anharmonic systems. This conclusion, however, is based only on SSCHA relaxations at 0 K for  $\text{H}_3\text{S}$  structures within a  $\sim$ 100 meV/atom enthalpy threshold on the classical landscape. In reality, some structures, for example, bcc-Ti or bcc-Zr, have enthalpies more than 100 meV/atom above the ground state at 0 K yet become stable at high temperatures. Such phases would likely be missed by this more efficient but more limited, enthalpy-filtered

approach. For these cases, a full anharmonic landscape search with SSCHA relaxations of high-energy structures remains necessary to correctly determine phase stability.

A structure search on the full quantum anharmonic free energy landscape can also benefit from its simplification compared to the classical landscape. To illustrate this, we performed DFT-based CSP on the classical energy landscape at 0 K (excluding ZPE) and 150 GPa using VASP. This search produced over twice as many diverse predicted polymorphs as the anharmonic search (even including false metastable polymorphs). Furthermore, the  $\text{LaH}_{10}$  with  $\text{Fm}\bar{3}\text{m}$  symmetry is not the most stable structure at 150 GPa. Structures with  $\text{Immm}$ ,  $\text{C}2$ ,  $\text{C}2/\text{m}$ ,  $\text{R}\bar{3}\text{m}$  and  $\text{Cm}$  space groups all have lower enthalpies than the  $\text{Fm}\bar{3}\text{m}$  phase at this pressure, that is contradict experimental findings [31].

The Figure 3 illustrates how the inclusion of quantum anharmonic effects reduces the number of viable  $\text{LaH}_{10}$  polymorphs. The comparison is made between a free-energy landscape at 300 K and a classical 0 K energy landscape, both generated via dimensionality reduction of fingerprint space using STMng [34]. While the projections are unique to each dataset, preventing a direct comparison, they clearly reveal the significant impact of anharmonic contributions on the structural search space. The simplified finite-temperature quantum anharmonic landscape offers a practical advantage in fields like superconducting hydride discovery by significantly reducing the number of candidate structures that require costly property calculations.

## 4. Conclusions

In this work, we have developed and demonstrated a CSP approach that incorporates quantum anharmonic effects into the search space through SSCHA accelerated with MLIPs. Using  $\text{LaH}_{10}$  at 150 GPa as a validation system, we show that:

1. **Lightweight local AL-MLIPs trained from scratch** enable accurate CSP on the anharmonic free-energy landscape when applying corrections from the thermodynamic perturbation theory, properly identifying the cubic  $\text{Fm}\bar{3}\text{m}$  phase of  $\text{LaH}_{10}$  as the ground state. Reusing lightweight local AL-MLIPs during CSP in the SSCHA relaxation reduces DFT cost significantly, though care must be taken to avoid accumulated errors and false metastable states.
2. **Large uMLIPs with millions of parameters**, such as Mattersim-5m, offer a promising alternative, nearly eliminating the need for system-specific training while maintaining robustness of SSCHA relaxations and providing correct structure ranking near the global minimum in the SSCHA-based CSP.
3. **Quantum anharmonicity critically simplifies the structural search space**, reducing the number of plausible polymorphs compared to classical 0 K landscapes. This simplification is particularly advantageous when there is a need to select structures for computationally expensive property evaluations in materials discovery.
4. **Full anharmonic CSP is necessary** to capture phases stabilized at finite temperatures, which may be missed by

enthalpy-filtered approaches based solely on 0 K energetics.

Our work paves the way for efficient, quantum-accurate CSP in strongly anharmonic systems, with direct implications for superconducting hydrides, thermoelectrics, and other quantum materials. Future efforts should focus on improving uMLIP accuracy for high-pressure systems and integrating more automated fine-tuning protocols within the CSP workflow.

## 5. Methods and computational details

### 5.1. Structure optimization within SSCHA using AL-MLIP

The structure optimization within the SSCHA is performed by minimizing the free-energy functional  $F[\mathcal{R}, \Phi]$  with respect to the centroid positions  $\mathcal{R}$  and the auxiliary force-constant matrix  $\Phi$ :

$$F = \min_{\mathcal{R}, \Phi} \mathcal{F}[\mathcal{R}, \Phi] = F[\mathcal{R}_{\text{eq}}, \Phi_{\text{eq}}]. \quad (1)$$

A schematic of the AL-MLIP workflow is shown in Figure 4. The optimization starts from an initial guess for  $\mathcal{R}$  and a trial density matrix  $\Phi$ , typically obtained from a 0 K relaxation and harmonic force constants computed either *ab initio* or with an MLIP.

Once  $\mathcal{R}$  and  $\Phi$  are initialized, an ensemble of displaced configurations is generated by sampling the Gaussian distribution defined by  $\Phi$  (typically in supercells). Energies, forces, and stresses are evaluated with the MLIP; if needed, representative candidates are recomputed with DFT, added to the training set, and the MLIP is retrained.

SSCHA then minimizes  $F[\mathcal{R}, \Phi]$  using a stochastic Monte Carlo approach (commonly with preconditioned gradient descent) until the free-energy gradients satisfy the convergence threshold [14, 15]. The output includes the temperature-dependent free energy, equilibrium positions, auxiliary force constants  $\Phi_{\text{eq}}$ , and stress tensor, incorporating quantum-thermal fluctuations and anharmonicity. Thermodynamic-perturbation corrections can be applied to bring the free energy closer to the *ab initio* level [7, 35–37].

Two points are worth emphasizing. First, a preliminary 0 K relaxation is crucial; otherwise, the harmonic dynamical matrix used to define  $\Phi$  may contain many imaginary frequencies, leading to an unphysically broad initial ionic distribution and unreliable energies, forces, and stresses.

Second, sufficiently large supercells are required to capture relevant phonon interactions, but the nonlinear scaling of SSCHA [14] makes large-supercell calculations expensive. We therefore use a multistage upscaling scheme. Stage 1 employs the smallest feasible supercell (or the primitive cell if it contains  $> 8$  atoms) to obtain  $\Phi$  and begin relaxation, enabling low-cost MLIP retraining if active learning is used. Stage 2 uses a medium supercell with periodic images of the atoms separated by more than one MLIP cutoff;  $\Phi$  is initialized by Fourier interpolation of the Stage 1 auxiliary dynamical matrix. Finally, with a well-trained MLIP, SSCHA proceeds in a sufficiently

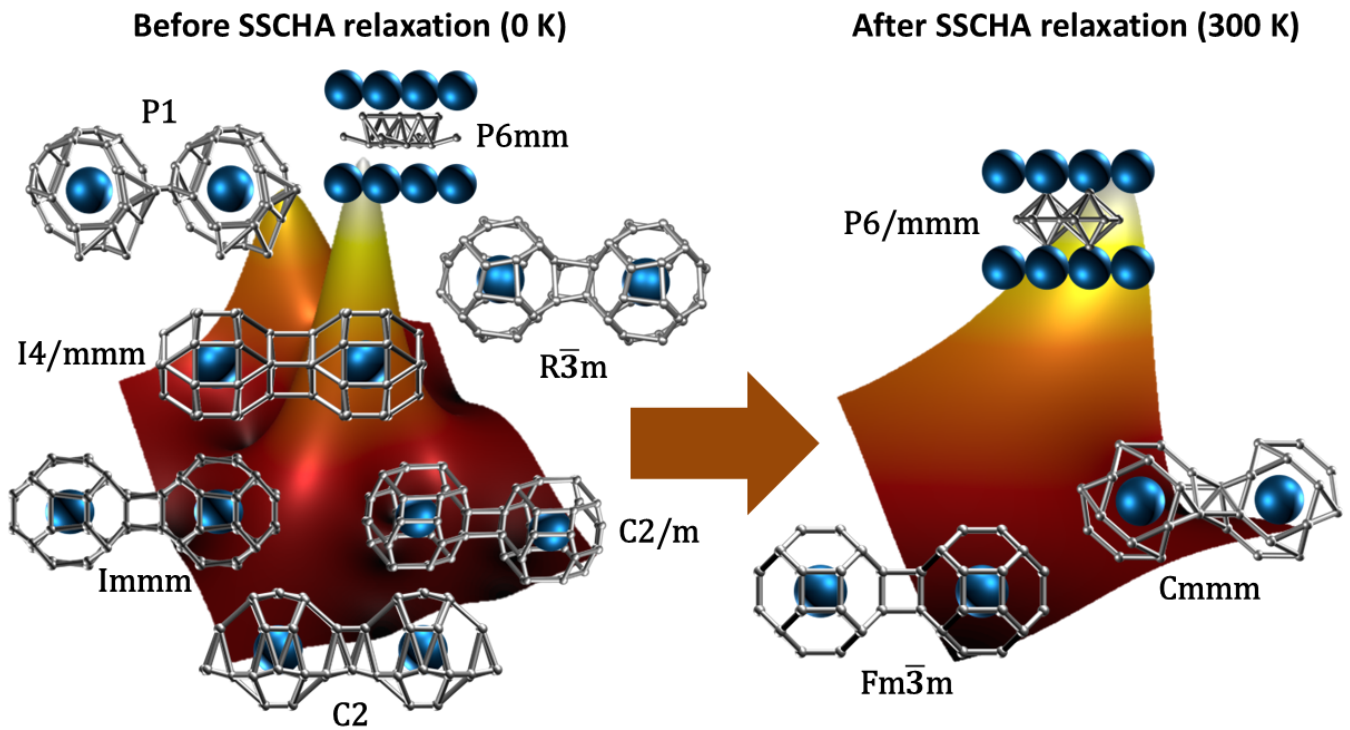


Figure 3: A comparison of energy landscapes showing the reduction in number of  $\text{LaH}_{10}$  polymorphs at 150 GPa when quantum anharmonicity is considered. The quantum anharmonic free-energy landscape at 300 K exhibits a simpler configuration space than the classical 0 K landscape. Both landscapes were generated using the dimensionality reduction method for fingerprint space implemented in STMng [34]. Although the projections are dataset-specific, they highlight the critical role of anharmonic effects in narrowing the search space during structural relaxation and ranking.

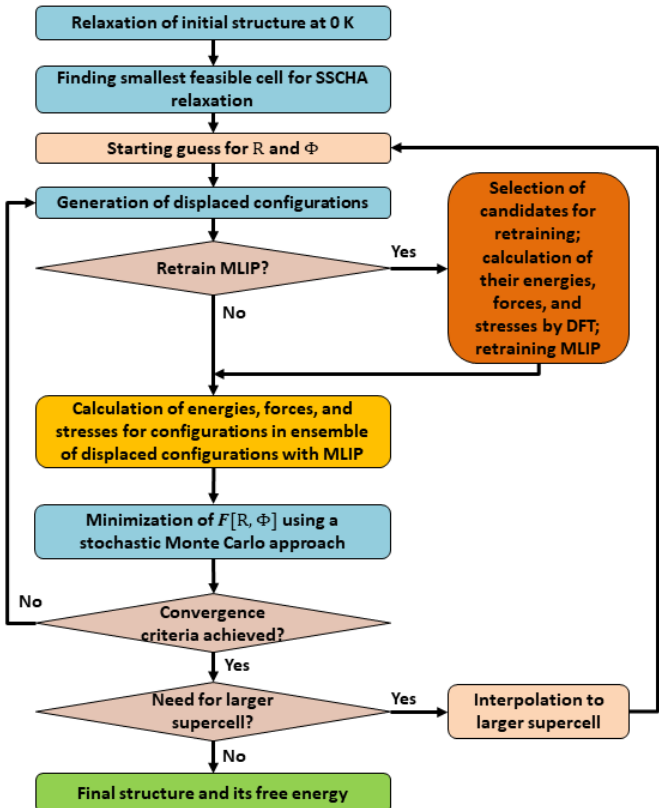


Figure 4: A common scheme of structure optimization within the SSCHA using active-learning MLIP.

large supercell using an interpolated  $\Phi$  from Stage 2; retraining is typically disabled and the main cost comes from MLIP evaluations and free-energy minimization.

This multistage strategy accelerates SSCHA relaxation relative to starting from a large supercell [16, 17].

### 5.2. Combining AL-MLIPs with SSCHA in structure prediction

The challenge of applying the AL scheme for MLIP outlined in the Figure 4 within the structure prediction is organizing this process in parallel, i.e. when several MLIPs are trained simultaneously. We therefore explored three strategies for applying AL-MLIPs in the SSCHA-based structure prediction.

**Strategy 1 (Local per-structure training):** For each new structure, a separate MLIP is trained from scratch on configurations from its SSCHA ensemble. While computationally feasible and allowing high-accuracy MLIPs tailored to each structure, this approach risks redundant DFT calculations for structures that existing MLIPs could already describe adequately.

**Strategy 2 (Global MLIP retraining):** A single global MLIP is retrained for each structure during a generation, then all retraining configurations are aggregated and the MLIP is retrained once per generation. This minimizes redundant DFT calculations but has a critical drawback: retraining global MLIPs (especially high-level MTPs) can demand more resources than the DFT calculations themselves. Details of this strategy's advantages and pitfalls are in Supplementary Materials.

**Strategy 3 (Hybrid: Reuse and retrain from existing MLIPs via MaxVol selection):** We propose a balanced approach. In the first bunch of structures treated in parallel, a separate MLIP is trained for each structure from scratch. All MLIPs then are stored. For the subsequent structures, a selection algorithm (MaxVol for MTPs) identifies which stored MLIP requires the fewest additional configurations for retraining. That MLIP is selected and retrained for the new structure. This allows reuse of MLIPs from promising (low-energy) structures, while less useful MLIPs are sidelined. The energy landscape is described piecewise by specialized MLIPs, and generalization errors from irrelevant structures do not degrade MLIPs for valuable ones. The drawback is that the number of local MLIPs grows with each generation; however, fast selection algorithms mitigate this.

In this work, we consider the results obtained with Strategy 1 for SSCHA-based structure prediction as a reference and completely discard Strategy 2 due to inefficiency.

### 5.3. Details of calculations

**Structure prediction.** In all cases, the fixed composition searches in unit cells with 11 atoms per cell were executed. The first generation of structures consisted from 30 candidates, while the subsequent generations consisted from 20 structures. In the first generation, structures were created only with random symmetry operator. Starting from second generation the soft mode mutation and heredity operators were added for structure creation. The searches were stopped if the most stable structure was not changed for 7 generations.

**AL-MLIP selection.** We used the moment tensor potentials (MTP) of level eight as AL-MLIPs. Our testing with MTPs of different levels revealed that training MTPs of eighth level from scratch for a particular structure allows to conduct its free energy minimization within the SSCHA preserving required accuracy at the moderate computational cost.

**DFT parameters.** The DFT calculations for training MLIPs and for the preliminary 0 K relaxations of structures were performed within the generalized gradient approximation (GGA) for the exchange-correlation (XC) energy with Perdew-Burke-Ernzerhof (PBE) parametrization [46] and standard projector augmented wave (PAW) [47] potentials for La and H elements as implemented in the Vienna Ab initio Simulation Package (VASP) [48]. The kinetic energy cutoff (500 eV) and k-points density ( $0.05 2\pi/\text{\AA}$ ) were chosen on the basis of the previous calculations of our group for this system [25] and additionally checked for convergence on harmonic phonon dispersion curves of cubic  $\text{LaH}_{10}$  with  $\text{Fm}\bar{3}\text{m}$  symmetry.

**SSCHA calculations.** We found that the convergence of the anharmonic free energy obtained at the end of the second and third stages of the upscaling SSCHA relaxation scheme is within  $\sim 2$  meV/atom for  $\text{LaH}_{10}$  structures selected for testing indicating the fast convergence of force constants with interatomic distance. For this reason, we allowed USPEX to use the results from the second stage to speed up the calculations.

For the  $\text{Fm}\bar{3}\text{m}$ ,  $\text{Cmmm}$ , and  $\text{P}6/\text{mmm}$   $\text{LaH}_{10}$  structures we performed additional SSCHA relaxations and Hessian calculations with actively learned MTPs of level 20 to obtain accurate phonon dispersions and check dynamical stability at harmonic and anharmonic level. The harmonic phonon dispersion was calculated with small displacement method [49] as implemented in the ASE package [50] using displacements of  $0.05 \text{ \AA}$ . The anharmonic phonon dispersion was calculated from the Hessian of the free energy, using the Stochastic Self-Consistent Harmonic Approximation (SSCHA) with ensemble of 100,000 configurations. Higher-order quartic corrections were found to be negligible and not included in the Hessian calculation. Both in harmonic and anharmonic cases the calculations were performed using  $2\times 2\times 2$  supercells.

## 6. Acknowledgments

This work was supported by the Russian Science Foundation (Grant No. 19-72-30043, <https://rscf.ru/project/19-72-30043/>).

## 7. Competing interests

The authors declare no competing interests.

## References

- [1] A. R. Oganov, C. W. Glass, Crystal structure prediction using ab initio evolutionary techniques: Principles and applications, *The Journal of Chemical Physics* 124 (24) (2006) 244704. doi:[10.1063/1.2210932](https://doi.org/10.1063/1.2210932).  
URL <http://aip.scitation.org/doi/10.1063/1.2210932>
- [2] a. R. Oganov, Y. Ma, a. O. Lyakhov, M. Valle, C. Gatti, Evolutionary Crystal Structure Prediction as a Method for the Discovery of Minerals and Materials, *Reviews in Mineralogy and Geochemistry* 71 (1) (2010) 271–298. doi:[10.2138/rmg.2010.71.13](https://doi.org/10.2138/rmg.2010.71.13).  
URL <http://rimg.geoscienceworld.org/cgi/doi/10.2138/rmg.2010.71.13>https://pubs.geoscienceworld.org/rimg/article/71/1/271-298/140855
- [3] L. M. Hunnisett, N. Francia, J. Nyman, N. S. Abraham, S. Aitipamula, T. Alkhidir, M. Almehairbi, A. Anelli, D. M. Anstine, J. E. Anthony, J. E. Arnold, F. Bahrami, M. A. Bellucci, G. J. O. Beran, R. M. Bhardwaj, R. Bianco, J. A. Bis, A. D. Boese, J. Bramley, D. E. Braun, P. W. V. Butler, J. Cadden, S. Carino, C. Červinka, E. J. Chan, C. Chang, S. M. Clarke, S. J. Coles, C. J. Cook, R. I. Cooper, T. Darden, G. M. Day, W. Deng, H. Dietrich, A. DiPasquale, B. Dhokale, B. P. van Eijck, M. R. J. Elsegood, D. Firaha, W. Fu, K. Fukuzawa, N. Galanakis, H. Goto, C. Greenwell, R. Guo, J. Harter, J. Helfferich, J. Hoja, J. Hone, R. Hong, M. Hušák, Y. Ikabata, O. Isayev, O. Ishaque, V. Jain, Y. Jin, A. Jing, E. R. Johnson, I. Jones, K. V. J. Jose, E. A. Kabova, A. Keates, P. F. Kelly, J. Klimeš, V. Kostková, H. Li, X. Lin, A. List, C. Liu, Y. M. Liu, Z. Liu, I. Lončarić, J. W. Lubach, J. Ludík, N. Marom, H. Matsui, A. Mattei, R. A. Mayo, J. W. Melkumov, B. Mladineo, S. Mohamed, Z. Momenzadeh Abardeh, H. S. Muddana, N. Nakayama, K. S. Nayal, M. A. Neumann, R. Nikhar, S. Obata, D. O'Connor, A. R. Oganov, K. Okuwaki, A. Otero-de-la Roza, S. Parkin, A. Parunov, R. Podeszwa, A. J. A. Price, L. S. Price, S. L. Price, M. R. Probert, A. Pulido, G. R. Ramteke, A. U. Rehman, S. M. Reutzel-Edens, J. Rogal, M. J. Ross, A. F. Rumson, G. Sadiq, Z. M. Saeed, A. Salimi, K. Sasikumar, S. Sekharan, K. Shankland, B. Shi, X. Shi, K. Shinohara, A. G. Skillman, H. Song, N. Strasser, J. van de Streek, I. J. Sugden, G. Sun, K. Szalewicz, L. Tan, K. Tang, F. Tarczynski, C. R. Taylor, A. Tkatchenko, R. Tom, P. Touš, M. E. Tuckerman, P. A. Unzueta, Y. Utsumi, L. Vogt-Maranto, J. Weatherston, L. J. Wilkinson, R. D. Willacy, L. Wojtas, G. R. Woollam, Y. Yang, Z. Yang, E. Yonemochi, X. Yue, Q. Zeng, T. Zhou, Y. Zhou, R. Zubatyuk, J. C. Cole, The seventh blind test of crystal structure prediction: structure ranking methods, *Acta Crystallographica Section B Structural Science, Crystal Engineering and Materials* 80 (6) (2024) 548–574. doi:[10.1107/S2052520624008679](https://doi.org/10.1107/S2052520624008679).  
URL <https://journals.iucr.org/paper?S2052520624008679>
- [4] K. Wang, X. Kong, J. Du, C. Li, Z. Li, Z. Wu, Thermodynamic description of the Ti–H system, *Calphad* 34 (3) (2010) 317–323. doi:[10.1016/j.calphad.2010.07.001](https://doi.org/10.1016/j.calphad.2010.07.001).  
URL <http://linkinghub.elsevier.com/retrieve/pii/S0364591610000465>

[5] A. Van der Ven, M. Aydinol, G. Ceder, G. Kresse, J. Hafner, First-principles investigation of phase stability in  $\text{Li}_{\text{x}}\text{CoO}_2$ , *Physical Review B* 58 (6) (1998) 2975–2987. doi:10.1103/PhysRevB.58.2975.  
URL <http://link.aps.org/doi/10.1103/PhysRevB.58.2975>

[6] L. Fiedler, N. A. Modine, S. Schmerler, D. J. Vogel, G. A. Popoola, A. P. Thompson, S. Rajamanickam, A. Cangi, Predicting electronic structures at any length scale with machine learning, *npj Computational Materials* 9 (1) (2023) 115. doi:10.1038/s41524-023-01070-z.  
URL <https://www.nature.com/articles/s41524-023-01070-z>

[7] I. A. Kruglov, A. V. Yanilkin, Y. Propad, A. B. Mazitov, P. Rachitskii, A. R. Oganov, Crystal structure prediction at finite temperatures, *npj Computational Materials* 9 (1) (2023) 197. doi:10.1038/s41524-023-01120-6.  
URL <https://www.nature.com/articles/s41524-023-01120-6>

[8] I. Errea, M. Calandra, F. Mauri, Huge anharmonic effects in superconducting hydrides and transition metal dichalcogenides, *physica status solidi (b)* 251 (12) (2014) 2556–2562. doi:10.1002/pssb.201451164.  
URL <https://onlinelibrary.wiley.com/doi/10.1002/pssb.201451164>

[9] I. Errea, M. Calandra, F. Mauri, Anharmonic free energies and phonon dispersions from the stochastic self-consistent harmonic approximation: Application to platinum and palladium hydrides, *Physical Review B* 89 (6) (2014) 064302. doi:10.1103/PhysRevB.89.064302.  
URL <https://link.aps.org/doi/10.1103/PhysRevB.89.064302>

[10] I. Errea, F. Belli, L. Monacelli, A. Sanna, T. Koretsune, T. Tadano, R. Bianco, M. Calandra, R. Arita, F. Mauri, J. A. Flores-Livas, Quantum crystal structure in the 250-kelvin superconducting lanthanum hydride, *Nature* 578 (7793) (2020) 66–69. doi:10.1038/s41586-020-1955-z.  
URL <http://www.nature.com/articles/s41586-020-1955-z>

[11] A. Meninno, I. Errea, Ab initio study of metastable occupation of tetrahedral sites in palladium hydrides and its impact on superconductivity, *arXiv* (2022) 1–9.  
URL <http://arxiv.org/abs/2209.14773>

[12] R. Bianco, I. Errea, L. Paulatto, M. Calandra, F. Mauri, Second-order structural phase transitions, free energy curvature, and temperature-dependent anharmonic phonons in the self-consistent harmonic approximation: Theory and stochastic implementation, *Physical Review B* 96 (1) (2017) 014111. doi:10.1103/PhysRevB.96.014111.  
URL <http://link.aps.org/doi/10.1103/PhysRevB.96.014111>

[13] N. Rivano, F. Libbi, C. W. Tan, C. Cheung, J. Lado, A. Mostofi, P. Kim, J. Lischner, A. O. Fumega, B. Kozinsky, Z. A. H. Goodwin, Exploring Charge Density Waves in two-dimensional  $\text{NbSe}_2$  with Machine Learning (2025) 1–10.  
URL <http://arxiv.org/abs/2504.13675>

[14] L. Monacelli, R. Bianco, M. Cherubini, M. Calandra, I. Errea, F. Mauri, The stochastic self-consistent harmonic approximation: calculating vibrational properties of materials with full quantum and anharmonic effects, *Journal of Physics: Condensed Matter* 33 (36) (2021) 363001. doi:10.1088/1361-648X/ac066b.  
URL <https://iopscience.iop.org/article/10.1088/1361-648X/ac066b>

[15] L. Monacelli, I. Errea, M. Calandra, F. Mauri, Pressure and stress tensor of complex anharmonic crystals within the stochastic self-consistent harmonic approximation, *Physical Review B* 98 (2) (2018) 024106. doi:10.1103/PhysRevB.98.024106.  
URL <https://doi.org/10.1103/PhysRevB.98.024106>  
<http://link.aps.org/doi/10.1103/PhysRevB.98.024106>

[16] R. Lucrezi, E. Kogler, S. Di Cataldo, M. Aichhorn, L. Boeri, C. Heil, Quantum lattice dynamics and their importance in ternary superhydride clathrates, *Communications Physics* 6 (1) (2023) 298. doi:10.1038/s42005-023-01413-8.  
URL <https://www.nature.com/articles/s42005-023-01413-8>

[17] F. Belli, E. Zurek, Efficient modelling of anharmonicity and quantum effects in  $\text{PdCuH}_2$  with machine learning potentials, *npj Computational Materials* 11 (1) (2025) 87. doi:10.1038/s41524-025-01553-1.  
URL <https://www.nature.com/articles/s41524-025-01553-1>

[18] K. T. Schütt, H. E. Sauceda, P.-J. Kindermans, A. Tkatchenko, K.-R. Müller, SchNet – A deep learning architecture for molecules and materials, *The Journal of Chemical Physics* 148 (24) (6 2018). doi:10.1063/1.5019779.  
URL <https://pubs.aip.org/jcp/article/148/24/241722/962591/SchNet-A-deep-learning-architecture-for-molecules>

[19] L. Ranalli, C. Verdi, L. Monacelli, G. Kresse, M. Calandra, C. Franchini, Temperature-Dependent Anharmonic Phonons in Quantum Paraelectric  $\text{KTaO}_3$  by First Principles and Machine-Learned Force Fields, *Advanced Quantum Technologies* 6 (4) (2023) 1–7. doi:10.1002/qute.202200131.  
URL <https://onlinelibrary.wiley.com/doi/10.1002/qute.202200131>

[20] W. Zhao, Y. Sun, J. Li, P. Yuan, T. Iitaka, X. Zhong, H. Li, Y.-W. Fang, H. Liu, I. Errea, Y. Xie, Exploring the Limits

of Superconductivity in Metal-Stuffed B-C Clathrates via Ionic Lattice Anharmonicity (2025) 1–8.  
 URL <http://arxiv.org/abs/2501.12068>

[21] J. Riebesell, R. E. Goodall, P. Benner, Y. Chiang, B. Deng, G. Ceder, M. Asta, A. A. Lee, A. Jain, K. A. Persson, A framework to evaluate machine learning crystal stability predictions, *Nature Machine Intelligence* 7 (6) (2025) 836–847. doi:10.1038/s42256-025-01055-1.  
 URL <http://dx.doi.org/10.1038/s42256-025-01055-1>

[22] H. Liu, I. I. Naumov, R. Hoffmann, N. W. Ashcroft, R. J. Hemley, Potential high- T c superconducting lanthanum and yttrium hydrides at high pressure, *Proceedings of the National Academy of Sciences* 114 (27) (2017) 6990–6995. doi:10.1073/pnas.1704505114.  
 URL <https://pnas.org/doi/full/10.1073/pnas.1704505114>

[23] F. Peng, Y. Sun, C. J. Pickard, R. J. Needs, Q. Wu, Y. Ma, Hydrogen Clathrate Structures in Rare Earth Hydrides at High Pressures: Possible Route to Room-Temperature Superconductivity, *Physical Review Letters* 119 (10) (2017) 107001. doi:10.1103/PhysRevLett.119.107001.  
 URL <https://link.aps.org/doi/10.1103/PhysRevLett.119.107001>

[24] H. Liu, I. I. Naumov, Z. M. Geballe, M. Somayazulu, J. S. Tse, R. J. Hemley, Dynamics and superconductivity in compressed lanthanum superhydride, *Physical Review B* 98 (10) (2018) 100102. doi:10.1103/PhysRevB.98.100102.  
 URL <https://doi.org/10.1103/PhysRevB.98.100102>  
<https://link.aps.org/doi/10.1103/PhysRevB.98.100102>

[25] I. A. Kruglov, D. V. Semenok, H. Song, R. Szcześniak, I. A. Wrona, R. Akashi, M. M. Davari Esfahani, D. Duan, T. Cui, A. G. Kvashnin, A. R. Oganov, Superconductivity of LaH<sub>10</sub> and LaH<sub>16</sub> polyhydrides, *Physical Review B* 101 (2) (2020) 024508. doi:10.1103/PhysRevB.101.024508.  
 URL <https://link.aps.org/doi/10.1103/PhysRevB.101.024508>

[26] K. K. Ly, D. M. Ceperley, Stability and distortion of fcc LaH<sub>10</sub> with path-integral molecular dynamics, *Physical Review B* 106 (5) (2022) 1–8. doi:10.1103/PhysRevB.106.054106.

[27] S. van de Bund, G. J. Ackland, Competition between superconductivity and molecularization in the quantum nuclear behavior of lanthanum hydride, *Physical Review B* 108 (18) (2023) 184102. doi:10.1103/PhysRevB.108.184102.  
 URL <https://link.aps.org/doi/10.1103/PhysRevB.108.184102>

[28] J. Guo, D. Semenok, G. Shutov, D. Zhou, S. Chen, Y. Wang, K. Zhang, X. Wu, S. Luther, T. Helm, X. Huang, T. Cui, Unusual metallic state in superconducting A15-type La4H23, *National Science Review* 11 (12) (2024) 1–10. doi:10.1093/nsr/nwae149.  
 URL <https://doi.org/10.1093/nsr/nwae149>  
<https://academic.oup.com/nsr/article/doi/10.1093/nsr/nwae149/7651283>

[29] Z. M. Geballe, H. Liu, A. K. Mishra, M. Ahart, M. Somayazulu, Y. Meng, M. Baldini, R. J. Hemley, Synthesis and Stability of Lanthanum Superhydrides, *Angewandte Chemie International Edition* 57 (3) (2018) 688–692. doi:10.1002/anie.201709970.  
 URL <https://onlinelibrary.wiley.com/doi/10.1002/anie.201709970>

[30] M. Somayazulu, M. Ahart, A. K. Mishra, Z. M. Geballe, M. Baldini, Y. Meng, V. V. Struzhkin, R. J. Hemley, Evidence for Superconductivity above 260 K in Lanthanum Superhydride at Megabar Pressures, *Physical Review Letters* 122 (2) (2019) 27001. doi:10.1103/PhysRevLett.122.027001.  
 URL <https://doi.org/10.1103/PhysRevLett.122.027001>

[31] A. P. Drozdov, P. P. Kong, V. S. Minkov, S. P. Besedin, M. A. Kuzovnikov, S. Mozaffari, L. Balicas, F. F. Balakirev, D. E. Graf, V. B. Prakapenka, E. Greenberg, D. A. Knyazev, M. Tkacz, M. I. Eremets, Superconductivity at 250 K in lanthanum hydride under high pressures, *Nature* 569 (7757) (2019) 528–531. doi:10.1038/s41586-019-1201-8.  
 URL <http://dx.doi.org/10.1038/s41586-019-1201-8>  
<https://www.nature.com/articles/s41586-019-1201-8>

[32] D. Sun, V. S. Minkov, S. Mozaffari, Y. Sun, Y. Ma, S. Chariton, V. B. Prakapenka, M. I. Eremets, L. Balicas, F. F. Balakirev, High-temperature superconductivity on the verge of a structural instability in lanthanum superhydride, *Nature Communications* 12 (1) (2021) 6863. doi:10.1038/s41467-021-26706-w.  
 URL <https://www.nature.com/articles/s41467-021-26706-w>

[33] D. Laniel, F. Trybel, B. Winkler, F. Knoop, T. Fedotenko, S. Khandarkhaeva, A. Aslandukova, T. Meier, S. Chariton, K. Glazyrin, V. Milman, V. Prakapenka, I. A. Abrikosov, L. Dubrovinsky, N. Dubrovinskaia, High-pressure synthesis of seven lanthanum hydrides with a significant variability of hydrogen content, *Nature Communications* 13 (1) (2022) 6987. doi:10.1038/s41467-022-34755-y.  
 URL <https://www.nature.com/articles/s41467-022-34755-y>

[34] M. Valle, STM3: A chemistry visualization platform, *Zeitschrift fur Kristallographie* 220 (5-6) (2005) 585–588. doi:10.1524/zkri.220.5.585.65068.

[35] L. Vočadlo, D. Alfè, Ab initio melting curve of the fcc phase of aluminum, *Physical Review B* 65 (21) (2002) 214105. doi:10.1103/PhysRevB.65.214105.  
URL <https://link.aps.org/doi/10.1103/PhysRevB.65.214105>

[36] L. Vočadlo, D. Alfè, G. D. Price, M. J. Gillan, Ab initio melting curve of copper by the phase coexistence approach, *The Journal of Chemical Physics* 120 (6) (2004) 2872–2878. doi:10.1063/1.1640344.  
URL <https://pubs.aip.org/jcp/article/120/6/2872/597257>  
`Ab-initio-melting-curve-of-copper-by-the-phase`

[37] A. R. Oganov, P. I. Dorogokupets, Intrinsic anharmonicity in equations of state and thermodynamics of solids, *Journal of Physics: Condensed Matter* 16 (8) (2004) 1351–1360. doi:10.1088/0953-8984/16/8/018.  
URL <https://iopscience.iop.org/article/10.1088/0953-8984/16/8/018>

[38] B. Deng, P. Zhong, K. Jun, J. Riebesell, K. Han, C. J. Bartel, G. Ceder, CHGNet as a pretrained universal neural network potential for charge-informed atomistic modelling, *Nature Machine Intelligence* 5 (9) (2023) 1031–1041. doi:10.1038/s42256-023-00716-3.  
URL <https://www.nature.com/articles/s42256-023-00716-3>

[39] D. Zhang, A. Peng, C. Cai, W. Li, Y. Zhou, J. Zeng, M. Guo, C. Zhang, B. Li, H. Jiang, T. Zhu, W. Jia, L. Zhang, H. Wang, A Graph Neural Network for the Era of Large Atomistic Models (2025) 1–28.  
URL <http://arxiv.org/abs/2506.01686>

[40] A. Bochkarev, Y. Lysogorskiy, R. Drautz, Graph Atomic Cluster Expansion for Semilocal Interactions beyond Equivariant Message Passing, *Physical Review X* 14 (2) (2024) 021036. doi:10.1103/PhysRevX.14.021036.  
URL <https://doi.org/10.1103/PhysRevX.14.021036>  
<https://link.aps.org/doi/10.1103/PhysRevX.14.021036>

[41] I. Batatia, P. Benner, Y. Chiang, A. M. Elena, D. P. Kovács, J. Riebesell, X. R. Advincula, M. Asta, M. Avaylon, W. J. Baldwin, F. Berger, N. Bernstein, A. Bhowmik, S. M. Blau, V. Cărare, J. P. Darby, S. De, F. Della Pia, V. L. Deringer, R. Eliošius, Z. El-Machachi, F. Falcioni, E. Fako, A. C. Ferrari, A. Genreith-Schriever, J. George, R. E. A. Goodall, C. P. Grey, P. Grigorev, S. Han, W. Handley, H. H. Heenen, K. Hermansson, C. Holm, J. Jaafar, S. Hofmann, K. S. Jakob, H. Jung, V. Kapil, A. D. Kaplan, N. Karimitari, J. R. Kermode, N. Kroupa, J. Kullgren, M. C. Kuner, D. Kuryla, G. Liepuoniute, J. T. Margraf, I.-B. Magdău, A. Michaelides, J. H. Moore, A. A. Naik, S. P. Niblett, S. W. Norwood, N. O'Neill, C. Ortner, K. A. Persson, K. Reuter, A. S. Rosen, L. L. Schaaf, C. Schran, B. X. Shi, E. Sivonxay, T. K. Stenczel, V. Svahn, C. Sutton, T. D. Swinburne, J. Tilly, C. van der Oord, E. Varga-Umbrich, T. Vegge, M. Vondrák, Y. Wang, W. C. Witt, F. Zills, G. Csányi, A foundation model for atomistic materials chemistry (3 2024).  
URL <http://arxiv.org/abs/2401.00096>

[42] H. Yang, C. Hu, Y. Zhou, X. Liu, Y. Shi, J. Li, G. Li, Z. Chen, S. Chen, C. Zeni, M. Horton, R. Pinsler, A. Fowler, D. Zügner, T. Xie, J. Smith, L. Sun, Q. Wang, L. Kong, C. Liu, H. Hao, Z. Lu, MatterSim: A Deep Learning Atomistic Model Across Elements, Temperatures and Pressures (2024) 1–86.  
URL <http://arxiv.org/abs/2405.04967>

[43] M. Neumann, J. Gin, B. Rhodes, S. Bennett, Z. Li, H. Choubisa, A. Hussey, J. Godwin, Orb: A Fast, Scalable Neural Network Potential (2024) 1–26.  
URL <http://arxiv.org/abs/2410.22570>

[44] J. Kim, J. Kim, J. Kim, J. Lee, Y. Park, Y. Kang, S. Han, Data-Efficient Multifidelity Training for High-Fidelity Machine Learning Interatomic Potentials, *Journal of the American Chemical Society* 147 (1) (2025) 1042–1054. doi:10.1021/jacs.4c14455.  
URL <https://pubs.acs.org/doi/10.1021/jacs.4c14455>

[45] H. Gao, Y.-w. Fang, I. Errea, Iterative learning scheme for crystal structure prediction with anharmonic lattice dynamics (2025) 1–26.  
URL <http://arxiv.org/abs/2512.20424>

[46] J. P. Perdew, K. Burke, M. Ernzerhof, Generalized Gradient Approximation Made Simple, *Physical Review Letters* 77 (18) (1996) 3865–3868. doi:10.1103/PhysRevLett.77.3865.  
URL <https://link.aps.org/doi/10.1103/PhysRevLett.77.3865>

[47] P. E. Blöchl, Projector augmented-wave method, *Physical Review B* 50 (24) (1994) 17953–17979. doi:10.1103/PhysRevB.50.17953.  
URL <https://link.aps.org/doi/10.1103/PhysRevB.50.17953>

[48] G. Kresse, J. Furthmüller, Efficiency of ab-initio total energy calculations for metals and semiconductors using a plane-wave basis set, *Computational Materials Science* 6 (1) (1996) 15–50. doi:10.1016/0927-0256(96)00008-0.  
URL <http://linkinghub.elsevier.com/retrieve/pii/0927025696000080>

[49] K.-M. Ho, C. Fu, B. Harmon, Vibrational frequencies via total-energy calculations. Applications to transition metals, *Physical Review B* 29 (4) (1984) 1575–1587. doi:10.1103/PhysRevB.29.1575.  
URL <https://link.aps.org/doi/10.1103/PhysRevB.29.1575>

[50] A. Hjorth Larsen, J. Jørgen Mortensen, J. Blomqvist, I. E. Castelli, R. Christensen, M. Dułak, J. Friis,

M. N. Groves, B. Hammer, C. Hargus, E. D. Hermes, P. C. Jennings, P. Bjerre Jensen, J. Kermode, J. R. Kitchin, E. Leonhard Kolsbjerg, J. Kubal, K. Kaasbjerg, S. Lysgaard, J. Bergmann Maronsson, T. Maxson, T. Olsen, L. Pastewka, A. Peterson, C. Rostgaard, J. Schiøtz, O. Schütt, M. Strange, K. S. Thygesen, T. Vegge, L. Vilhelmsen, M. Walter, Z. Zeng, K. W. Jacobsen, The atomic simulation environment—a Python library for working with atoms, *Journal of Physics: Condensed Matter* 29 (27) (2017) 273002. doi:10.1088/1361-648X/aa680e.

URL <https://iopscience.iop.org/article/10.1088/1361-648X/aa680e>